New Noncentrosymmetric Vanadates $Sr_9R(VO_4)_7$ (R = Tm, Yb, and Lu): Synthesis, Structure Analysis, and Characterization

Alexei A. Belik,*[,†,‡] Mikio Takano,[†] Mikhail V. Boguslavsky,[§] Sergey Yu. Stefanovich,[§,||] and Bogdan I. Lazoryak[§]

Institute for Chemical Research, Kyoto University, Uji, Kyoto-fu 611-0011, Japan, PRESTO, Japan Science and Technology Agency (JST), Kawaguchi, Saitama 332-0012, Japan, Department of Chemistry, Moscow State University, Moscow 119992, Russia, and State Scientific Center, Karpov Institute of Physical Chemistry, Moscow 103063, Russia

Received September 30, 2004. Revised Manuscript Received October 28, 2004

New vanadates $Sr_9R(VO_4)_7$ (R = Tm, Yb, and Lu) were synthesized using a standard solid-state method at 1373 K and found to be isotypic with $Ca_3(VO_4)_2$ at room temperature (RT). Their structure parameters were refined using the Rietveld method from synchrotron X-ray diffraction (XRD) data measured at RT (space group $R3c$ and $Z = 6$). $Sr_9R(VO_4)_7$ (R = Y and La−Er) do not form a phase isotypic with $Ca_3(VO_4)_2$. $Sr_9R(VO_4)_7$ (R = Tm, Yb, and Lu) were characterized through the magnetic susceptibility (2−400 K), the specific heat (0.45−31 K), thermal analysis (300−1573 K), and high-temperature XRD, second-harmonic generation, and dielectric measurements. The temperature dependence of the dielectric constant and tangent loss suggested that they exhibit a reversible ferroelectric−paraelectric phase transition of the first order near 950−960 K. The high-temperature phases have space group $R\bar{3}m$ and $Z = 3$. Thermal analysis revealed the presence of an intermediate phase between the $R3c$ and $R\bar{3}m$ phases in a very narrow temperature range. Magnetic susceptibilities of $Sr_9Tm(VO_4)_7$ and $Sr_9Yb(VO_4)_7$ are typical of Tm^{3+} and Yb^{3+} ions affected by an octahedral crystal field. The effective magnetic moments were 7.39 μ_B for Tm^{3+} and 4.59 μ_B for Yb^{3+}.

1. Introduction

Vanadates $M_3(VO_4)_2$ (M = Ca, Sr, and Ba) have attracted much attention owing to their interesting dielectric,[1] transport,[2−4] and optical[5−7] properties. They exhibit intense luminescence when activated with rare-earth metals or doped with Mn^{5+} ions and can be used as luminophors and host materials for lasers.

$Ca_3(VO_4)_2$ (space group $R3c$, $Z = 21$, $a = 10.809$ Å, and $c = 38.028$ Å)[8] is a high-temperature ferroelectric with $T_c = 1383$ K,[1] and it has additional anomalies in Raman scattering spectra,[7] dielectric properties, and electronic thermal emission spectra at 550−800 K. Vanadates $Ca_9R(VO_4)_7$ with R = Y, La−Lu, and Bi (space group $R3c$, $Z = 6$), which are isotypic with $Ca_3(VO_4)_2$, also show ferroelectric phase transitions at $T_c \approx 1070-1200$ K.[9] In addition, they demonstrate large second-harmonic generation efficiency, especially $Ca_9Bi(VO_4)_7$ (about 140 times as large as that of quartz).[9,10]

$Ca_3(VO_4)_2$ is isotypic with β-$Ca_3(PO_4)_2$. $Sr_3(VO_4)_2$ and $Ba_3(VO_4)_2$ as well as their phosphorus analogues have the $K_2Pb(SO_4)_2$ palmierite structure and belong to space group $R\bar{3}m$ ($a = 5.619$ Å, $c = 20.100$ Å, and $Z = 3$ for $Sr_3(VO_4)_2$).[11] Solid solutions of $Ca_{3-x}Sr_x(VO_4)_2$ with the structure of $Ca_3(VO_4)_2$ are formed in the compositional range of $0 \le x \le 1.5$,[12] while solid solutions of $Ca_{3-x}Sr_x(PO_4)_2$ with the β-$Ca_3(PO_4)_2$-type structure have a longer extension with $0 \le x \le 2.31$.[13] Strontium phosphates with the β-$Ca_3(PO_4)_2$-related structures can be stabilized by different cations, e.g., $Sr_9R(PO_4)_7$ (R = Sc, Cr, Fe, Ga, Y, In, and Gd−Lu),[14,15] $Sr_{9.3}Ni_{1.2}(PO_4)_7$,[16] $Sr_9NiLi(PO_4)_7$, $Sr_{9.04}Ni_{1.02}$-

* To whom correspondence should be addressed. Present address: International Center for Young Scientists, National Institute for Materials Science, Namiki 1-1, Tsukuba, Ibaraki 305-0044, Japan. Phone: +81 (029) 851-3354 (ext 8587). Fax: +81 (029) 860-4706. E-mail: alexei.belik@nims.go.jp.
† Kyoto University.
‡ JST.
§ Moscow State University.
|| Karpov Institute of Physical Chemistry.

(1) Glass, A. M.; Abrahams, S. C.; Ballmann, A. A.; Loiacono, G. *Ferroelectrics* **1978**, *17*, 579.
(2) Leonidov, I. A.; Belik, A. A.; Leonidova, O. N.; Lazoryak, B. I. *Russ. J. Inorg. Chem.* **2002**, *47*, 305.
(3) Leonidov, I. A.; Dontsov, G. I.; Knyazhev, A. S.; Slinkina, M. V.; Leonidova, O. N.; Fotiev, A. A. *Russ. J. Electrochem.* **1999**, *35*, 29.
(4) Leonidov, I. A.; Leonidova, O. N.; Fotiev, A. A. *Sov. Electrochem.* **1992**, *28*, 1241.
(5) Buijsse, B.; Schmidt, J.; Chan, I. Y.; Singel, D. J. *Phys. Rev. B* **1995**, *51*, 6215.
(6) Merkle, L. D.; Pinto, A.; Verdun, H. R.; McIntosh, B. *Appl. Phys. Lett.* **1992**, *61*, 2386.
(7) Grzechnik, A. *Chem. Mater.* **1998**, *10*, 1034.
(8) Gopal, R.; Calvo, C. *Z. Kristallogr.* **1973**, *137*, 67.
(9) (a) Lazoryak, B. I.; Belik, A. A.; Stefanovich, S. Yu.; Morozov, V. A.; Malakho, A. P.; Baryshnikova, O. V.; Leonidov, I. A.; Leonidova, O. N. *Dokl. Phys. Chem.* **2002**, *384*, 144; translated from *Dokl. Akad. Nauk* **2002**, *384*, 780. (b) Lazoryak, B. I.; Baryshnikova, O. V.; Stefanovich, S. Yu.; Malakho, A. P.; Morozov, V. A.; Belik, A. A.; Leonidov, I. A.; Leonidova, O. N.; Van Tendeloo, G. *Chem. Mater.* **2003**, *15*, 3003.
(10) Evans, J. S. O.; Huang, J.; Sleight, A. W. *J. Solid State Chem.* **2001**, *157*, 255.
(11) Carrillo-Cabrera, W.; von Schnering, G. H. *Z. Kristallogr.* **1993**, *205*, 271.
(12) Belik, A. A.; Stefanovich, S. Y.; Lazoryak, B. I. *Mater. Res. Bull.* **2001**, *36*, 1873.
(13) Belik, A. A.; Izumi, F.; Stefanovich, S. Yu.; Malakho, A. P.; Lazoryak, B. I.; Leonidov, I. A.; Leonidova, O. N.; Davydov, S. A. *Chem. Mater.* **2002**, *14*, 3197.

10.1021/cm048282f CCC: $30.25
Published on Web 12/13/2004

$Na_{0.88}(PO_4)_7$, and $Sr_{9.04}Ni_{1.04}K_{0.76}(PO_4)_7$.[17] Note that $Sr_{9.04}Ni_{1.02}Na_{0.88}(PO_4)_7$ and $Sr_{9.04}Ni_{1.04}K_{0.76}(PO_4)_7$ (space group $R3c$ and $Z = 6$) are isotypic with β-$Ca_3(PO_4)_2$.[17]

In this work, we have studied vanadates with the nominal composition of $Sr_9R(VO_4)_7$ (R = Y and La−Lu). We have shown that $Sr_9R(VO_4)_7$ (R = Tm, Yb, and Lu) are isotypic with $Ca_3(VO_4)_2$ and refined their structure parameters using synchrotron X-ray powder diffraction data. We have characterized them using the magnetic susceptibility, the specific heat, thermal analysis, and high-temperature X-ray powder diffraction, second-harmonic generation, and dielectric measurements. The observed characteristic anomalies on the dielectric data suggested that a ferroelectric−paraelectric phase transition of the first order takes place at 950−960 K in $Sr_9R(VO_4)_7$ (R = Tm, Yb, and Lu).

2. Experimental Section

Synthesis. Vanadates with the nominal composition of $Sr_9R(VO_4)_7$ (R = Y and La−Lu) were prepared using a usual solid-state method from stoichiometric mixtures of $SrCO_3$ (99.99%), V_2O_5 (99.9%), R_2O_3 (R = Y, La, Nd−Gd, and Dy−Lu), Pr_6O_{11}, and Tb_4O_7. The mixtures were placed in alumina crucibles and heated at 953 K for 30 h. They were then reground and treated at different temperatures ranging from 1273 to 1473 K with several intermediate grindings. Pt crucibles were used for heating above 1323 K. $Sr_9R(VO_4)_7$ (R = Tm, Yb, and Lu) were synthesized by heating appropriate mixtures in Pt crucibles at 1373 K for 150 h with four intermediate grindings and finally cooling in the furnace. They were light yellow.

X-ray Powder Diffraction (XRD) Procedures. Laboratory XRD data for phase analysis at room temperature (RT) and high-temperature XRD data were collected with a Rigaku RINT 2500 diffractometer (2θ range of 8−100°, a step width of 0.02°, and a counting time of 1 s/step). In high-temperature XRD experiments, the heating rate was 10 K/min. Mass fractions of impurities in the samples were estimated from the scale factors refined in their Rietveld analyses.

Synchrotron XRD data of $Sr_9R(VO_4)_7$ (R = Tm, Yb, and Lu) were measured at RT on a powder diffractometer, BL02B2 (with the Debye−Scherrer geometry), at SPring-8.[18] The samples were contained in glass (or quartz) capillary tubes with an inner diameter of 0.2 mm and rotated during the measurements. The data were collected with $\lambda \approx 0.776$ Å in a 2θ range from 1° to 74° with a step interval of 0.01°. We also collected high-temperature synchrotron XRD data. The samples were heated to the desired temperature in 2−3 min.

Structure parameters were refined with the Rietveld method using RIETAN-2000.[19] The split pseudo-Voigt function of Toraya[20] was used as a profile function. The background was represented by a composite background function, i.e., an 11th-order Legendre polynomial multiplied by a set of numerical values to approximate the background. The coefficients for analytical approximation to the atomic scattering factors for Sr, Tm, Yb, Lu, V, and O were taken from ref 21. The isotropic Debye−Waller factors represented as $\exp((-8\pi^2 U \sin^2\theta)/\lambda^2)$ were assigned to all the sites, where U is the isotropic atomic displacement parameter. Partial profile relaxation[19] was applied to (0,1,2), (1,0,4), (2,1,4), (0,2,10), and (2,2,0) reflections to improve fits in these reflections in the last stages of the structure refinements.

Thermal Analysis. Thermogravimetry (TG) and differential thermal analysis (DTA) of $Sr_9R(VO_4)_7$ (R = Tm, Yb, and Lu) were carried out in the air with a MacScience TG-DTA 2000 instrument. The samples were placed in Pt crucibles, heated to 1273 K, and cooled to RT at a rate of 10 K/min in the first cycle and at 5 K/min in the second cycle. After this procedure, they remained single-phased as examined with XRD. In another run of the TG and DTA experiments, the samples were heated to 1573 K and cooled to RT at 10 K/min (one cycle). The samples also remained single-phased after this run.

Physical Characterization. Second-harmonic generation (SHG) responses of powder samples (grain size of about 3 μm) were measured in a reflection scheme using a Q-switch pulsed YAG:Nd laser operated at a wavelength, λ_ω, of 1064 nm. The SHG signals were registered in reference to α-SiO_2 (grain size 3−5 μm) kept at RT. The temperature dependence of the SHG signals of the samples was measured between 300 and 1000 K.[13,17]

To measure the dielectric permittivity (ϵ) and loss tangent (tan δ) of $Sr_9R(VO_4)_7$ (R = Tm, Yb, and Lu), we used samples in the form of pellets (~1 mm in thickness and ~5 mm in diameter). They were pelletized at 200 kgf/cm^2 and then sintered at 1373 K for 30 h. A Pt paste was put on flat surfaces of the pellets, and then they were heated to 923 K to produce metal electrodes. ϵ and tan δ were registered with computer-controlled ac bridges R5083 and E7-12 at electric-field frequencies between 1 kHz and 1 MHz in a temperature range of 300−1070 K.

Magnetic susceptibilities, $\chi = \mathbf{M}/\mathbf{H}$, of $Sr_9Tm(VO_4)_7$ and $Sr_9Yb(VO_4)_7$ were measured on a dc SQUID magnetometer (Quantum Design, MPMS XL) between 2 and 400 K in an applied field of 100 Oe under both zero-field-cooled (ZFC) and field-cooled (FC) conditions. Specific heat capacities, C_p, were recorded between 0.45 and 31 K (on cooling) by a pulse relaxation method using a commercial calorimeter (Quantum Design, PPMS).

3. Results and Discussion

The samples with the nominal composition of $Sr_9R(VO_4)_7$ (R = Y and La−Er) were single-phased and isotypic with $Sr_3(VO_4)_2$ (space group $R\bar{3}m$)[11] or contained a phase isotypic with $Sr_3(VO_4)_2$ plus RVO_4, depending on the annealing conditions and the R^{3+} ion size (see the Supporting Information). The extension of solid solutions $Sr_{3-1.5x}R_x(VO_4)_2$ with the structure of $Sr_3(VO_4)_2$ increased with increasing synthesis temperature and increasing R^{3+} ion size. For example, single-phased samples with the nominal composition of $Sr_9R(VO_4)_7$ (corresponding to $x \approx 0.286$) could be prepared for R = La−Eu at 1273−1473 K. It is known that solid solutions $Sr_{3-1.5x}La_x(VO_4)_2$ are formed in the compositional range of

(14) Belik, A. A.; Izumi, F.; Ikeda, T.; Okui, M.; Malakho, A. P.; Morozov, V. A.; Lazoryak, B. I. *J. Solid State Chem.* **2002**, *168*, 237.
(15) Belik, A. A.; Izumi, F.; Ikeda, T.; Lazoryak, B. I.; Morozov, V. A.; Malakho, A. P.; Stefanovich, S. Yu.; Grebenev, V. V.; Shelmenkova, O. V.; Kamiyama, T.; Oikawa, K.; Leonidov, I. A.; Leonidova, O. N.; Davydov, S. A. *Phosphorus, Sulfur, Silicon Relat. Elem.* **2002**, *177*, 1899.
(16) Belik, A. A.; Izumi, F.; Ikeda, T.; Morozov, V. A.; Dilanian, R. A.; Torii, S.; Kopnin, E. M.; Lebedev, O. I.; Van Tendeloo, G.; Lazoryak, B. I. *Chem. Mater.* **2002**, *14*, 4464.
(17) Belik, A. A.; Izumi, F.; Ikeda, T.; Malakho, A. P.; Lazoryak, B. I. *J. Mater. Chem.* **2002**, *12*, 3803.
(18) Nishibori, E.; Takata, M.; Kato, K.; Sakata, M.; Kubota, Y.; Aoyagi, S.; Kuroiwa, Y.; Yamakata, M.; Ikeda, N. *Nucl. Instrum. Methods Phys. Res., Sect. A* **2001**, *467−468*, 1045.
(19) Izumi, F.; Ikeda, T. *Mater. Sci. Forum* **2000**, *321−324*, 198.
(20) Toraya, H. *J. Appl. Crystallogr.* **1990**, *23*, 485.
(21) *International Tables for Crystallography*, 2nd ed.; Wilson, A. J. C., Prince, E., Eds.; Kluwer: Dordrecht, The Netherlands, 1999; Vol. C, pp 572−574.

Table 1. Conditions of the Synchrotron XRD Experiments and Parts of the Refinement Results for $Sr_9R(VO_4)_7$ (R = Tm, Yb, and Lu)

	$Sr_9Tm(VO_4)_7$	$Sr_9Yb(VO_4)_7$	$Sr_9Lu(VO_4)_7$
wavelength (Å)	0.77572	0.77619	0.77619
capillary tube	quartz	quartz	glass
used 2θ range (deg)	4−74	4−74	4−74
scan width (deg)	0.01	0.01	0.01
space group	*R*3*c* (No. 161)	*R*3*c* (No. 161)	*R*3*c* (No. 161)
Z	6	6	6
lattice parameters			
a (Å)	11.19964(6)	11.19856(7)	11.20162(6)
c (Å)	39.8111(2)	39.7662(2)	39.7489(2)
V (Å^3)	4324.57(4)	4318.86(4)	4319.34(4)
no. of Bragg reflns	1891	1887	1886
ionic radius of the R^{3+} ion in 6-fold coordination (Å)[30]	0.880	0.868	0.861
variables			
structure; lattice	61; 2	61; 2	61; 2
background; profile	12; 6	12; 6	12; 6
peak shift; scale	1; 1	1; 1	1; 1
PPP[a]	25	25	25
R_{wp} (%); R_p (%)	2.14; 1.56	2.31; 1.78	2.24; 1.68
R_B (%); R_F (%)	1.67; 1.07	1.60; 0.85	0.91; 0.73
$S = R_{wp}/R_e$	1.09	1.48	1.50

[a] Refined primary profile parameter (PPP).[19]

$0 \le x \le 2/3$.[22] The La-rich boundary corresponds to the composition of $Sr_3La(VO_4)_3$.

On the other hand, the samples with the nominal composition of $Sr_9R(VO_4)_7$ and R = Tm, Yb, and Lu were found to be isotypic with $Ca_3(VO_4)_2$. They were monophasic. The structure parameters of $Ca_3(VO_4)_2$[8] were used as the initial ones in the Rietveld refinements of $Sr_9R(VO_4)_7$ (R = Tm, Yb, and Lu). The Ca^{2+} ions occupy the M1 (18*b*; $x \approx 0.72$, $y \approx 0.86$, and $z \approx 0.43$), M2 (18*b*; $x \approx 0.61$, $y \approx 0.83$, and $z \approx 0.23$), and M3 (18*b*; $x \approx 0.12$, $y \approx 0.27$, and $z \approx 0.32$) sites in $Ca_3(VO_4)_2$. In $Sr_9R(VO_4)_7$ (R = Tm, Yb, and Lu), these three sites were fully occupied by Sr^{2+} ions, i.e., g(Sr) = 1 for the M1−M3 sites, where g denotes the occupancy. The R^{3+} ions were located at the octahedral M5 site (6*a*; $z = 0$) with g(R) = 1. The Rietveld analyses with the above model afforded sufficiently low *R* factors and reasonable *U* parameters for all the sites. The M4 site (6*a*; $z \approx 0.18$), half-occupied by Ca^{2+} ions in $Ca_3(VO_4)_2$, was found to be vacant in $Sr_9R(VO_4)_7$ (R = Tm, Yb, and Lu). For example, the refinement of g(M4) for $Sr_9Yb(VO_4)_7$ resulted in g(Sr) = −0.004(4) with fixed $U = 0.02$ Å.

Figure 1 shows the experimental, calculated, and difference synchrotron XRD patterns for $Sr_9Yb(VO_4)_7$ as an example. Table 1 lists experimental and refinement conditions, final *R* factors, lattice parameters, and so forth. The final fractional coordinates and *U* values are listed in Table 2, where the M1, M2, M3, and M5 sites are denoted as Sr1, Sr2, Sr3, and Ln, respectively. Selected bond lengths appear in Table 3.

The Sr atoms in $Sr_9R(VO_4)_7$ (R = Tm, Yb, and Lu) are located at sites with 8-fold (Sr1 and Sr2) and 9-fold (Sr3) coordinations. The Sr3 site has the largest coordination number, but the Sr3 atoms are still underbonded as estimated through bond valence sum (BVS)[23] calculations (see Table 3). The atoms at the M3 site were found to be underbonded in other $Ca_3(VO_4)_2$-type compounds also.[10] BVS for the Sr1 and Sr2 sites was close to the expected value of 2.0. The

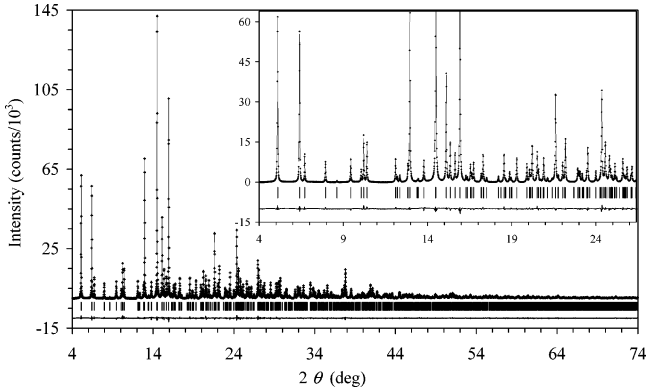

Figure 1. Observed (plus signs), calculated (solid line), and difference synchrotron XRD patterns of $Sr_9Yb(VO_4)_7$ at room temperature. Tick marks denote the peak positions of possible Bragg reflections. Background intensities were subtracted from the observed and calculated intensities. The inset presents an enlarged fragment of this figure.

R^{3+} ions occupy the small octahedral site, M5, with an average M5−O distance of 2.21 Å. The Sr^{2+} and R^{3+} ions are completely ordered in $Sr_9R(VO_4)_7$ (R = Tm, Yb, and Lu) in contrast to the case of $Ca_9R(VO_4)_7$ (R = Y and La−Lu).[24] In $Ca_9R(VO_4)_7$, La^{3+}−Eu^{3+} ions are distributed among the M1, M2, and M3 sites together with Ca^{2+} ions, whereas Y^{3+} and Tb^{3+}−Lu^{3+} ions occupy the M1, M2, and M5 sites together with Ca^{2+} ions. The M5 site is partially occupied by R^{3+} ions starting from Tb^{3+}, and the occupation of the M5 site in $Ca_9Lu(VO_4)_7$ is g(Ca) = 0.5 and g(Lu) = 0.5.[24]

$Sr_9R(VO_4)_7$ (R = Y and Tb−Er) with the $Ca_3(VO_4)_2$-type structure could not be obtained. This fact can be explained in terms of the increase in stress at the M5 site with increasing R^{3+} radius. The average M5−O distance is the same in $Sr_9R(VO_4)_7$ (R = Tm, Yb, and Lu). We may assume that the whole framework does not allow the M5 site to expand further in these compounds. BVS for the M5 site in $Sr_9R(VO_4)_7$ (R = Tm, Yb, and Lu) is larger than the expected value of 3.0 especially in $Sr_9Tm(VO_4)_7$ (BVS = 3.37 for M5). With the same M5−O distances as those of Sr_9Tm-

(22) Skakle, J. M. S.; Coats, A. M.; Marr, J. *J. Mater. Sci.* **2000**, *35*, 3251.
(23) Brese, N. E.; O'Keeffe, M. *Acta Crystallogr., Sect. B: Struct. Sci.* **1991**, *47*, 192.
(24) Belik, A. A.; Grechkin, S. V.; Dmitrienko, L. O.; Morozov, V. A.; Khasanov, S. S.; Lazoryak, B. I. *Crystallogr. Rep.* **2000**, *45*, 896.

Table 2. Fractional Coordinates and Isotropic Atomic Displacement Parameters for $Sr_9R(VO_4)_7$ (R = Tm, Yb, and Lu)[a]

site	Wyckoff position	*x*	*y*	*z*	10^2U (Å^2)
Sr1	18*b*	0.7206(3)	0.8585(4)	0.43239(9)	1.36(7)
		0.7225(2)	0.8582(2)	0.43253(5)	1.30(4)
		0.72171(15)	0.8569(2)	0.43263(4)	1.31(3)
Sr2	18*b*	0.6196(3)	0.8244(4)	0.23263(8)	1.45(9)
		0.6197(2)	0.8240(2)	0.23233(5)	1.09(5)
		0.61937(13)	0.8228(2)	0.23222(4)	1.37(4)
Sr3	18*b*	0.1307(4)	0.2767(2)	0.32546(8)	1.95(7)
		0.1295(2)	0.27521(12)	0.32525(5)	1.43(4)
		0.1295(2)	0.27542(9)	0.32524(4)	1.59(3)
Ln = Tm	6*a*	0	0	0	1.17(4)
Ln = Yb		0	0	0	0.73(2)
Ln = Lu		0	0	0	0.82(2)
V1	6*a*	0	0	0.27169(14)	1.75(14)
		0	0	0.27159(8)	1.06(8)
		0	0	0.27118(7)	1.28(6)
V2	18*b*	0.6823(3)	0.8583(5)	0.13377(14)	0.51(13)
		0.6853(2)	0.8586(3)	0.13487(7)	0.36(8)
		0.6845(2)	0.8580(2)	0.13480(6)	0.42(6)
V3	18*b*	0.6529(5)	0.8432(6)	0.03129(14)	1.36(16)
		0.6562(3)	0.8454(4)	0.03203(8)	0.95(8)
		0.6546(2)	0.8442(3)	0.03178(6)	1.11(7)
O1	6*a*	0	0	0.3146(5)	1.1(5)
		0	0	0.3138(3)	2.4(4)
		0	0	0.3135(2)	1.4(3)
O2	18*b*	0.0139(15)	0.8616(11)	0.2572(4)	2.7(5)
		0.0161(7)	0.8626(6)	0.2600(2)	0.5(2)
		0.0167(6)	0.8630(5)	0.25973(15)	1.1(2)
O3	18*b*	0.7263(16)	0.9014(17)	0.1744(4)	3.0(5)
		0.7306(9)	0.9070(9)	0.1741(2)	1.9(3)
		0.7329(7)	0.9087(7)	0.1739(2)	1.8(2)
O4	18*b*	0.7540(17)	0.7590(17)	0.1223(4)	0.8(5)
		0.7550(10)	0.7625(11)	0.1215(2)	0.6(3)
		0.7559(9)	0.7631(9)	0.1211(2)	0.8(2)
O5	18*b*	0.7319(20)	0.0072(16)	0.1130(4)	1.2(5)
		0.7240(12)	0.0066(9)	0.1129(2)	1.0(3)
		0.7224(10)	0.0016(8)	0.1121(2)	1.9(3)
O6	18*b*	0.5058(14)	0.7603(23)	0.1317(4)	1.4(4)
		0.5059(9)	0.7543(14)	0.1296(3)	1.2(3)
		0.5041(7)	0.7578(11)	0.1312(2)	0.9(2)
O7	18*b*	0.6002(19)	0.9456(19)	0.0460(5)	1.9(5)
		0.6036(11)	0.9504(11)	0.0454(3)	1.6(3)
		0.6013(8)	0.9512(8)	0.0453(2)	0.6(2)
O8	18*b*	0.5854(18)	0.6894(19)	0.0502(5)	3.1(6)
		0.5838(10)	0.6853(10)	0.0511(3)	0.8(3)
		0.5833(8)	0.6859(9)	0.0509(2)	1.5(3)
O9	18*b*	0.8293(14)	0.9202(24)	0.0384(4)	0.6(4)
		0.8311(9)	0.9179(14)	0.0371(2)	0.2(2)
		0.8297(7)	0.9200(12)	0.0379(2)	0.5(2)
O10	18*b*	0.6177(13)	0.8145(21)	0.9906(3)	1.2(3)
		0.6202(7)	0.8194(12)	0.9901(2)	0.9(2)
		0.6198(6)	0.8175(9)	0.99028(14)	0.75(15)

[a] For each site, the first line of columns *x*, *y*, *z*, and *U* is for $Sr_9Tm(VO_4)_7$, the second one is for $Sr_9Yb(VO_4)_7$, and the third one is for $Sr_9Lu(VO_4)_7$. The occupancies of all the sites are 1.

$(VO_4)_7$, we obtain BVS = 3.46 for Er^{3+} ions.[23] The presence of such an overbonded unstable site leads to the collapse of the $Ca_3(VO_4)_2$-type structure for R^{3+} ions larger than Tm^{3+}. In $Ca_9R(VO_4)_7$ (R = Y and Tb−Lu), the stress at the M5 site is relieved by the partial occupation by Ca^{2+} ions. Note that phosphates $Sr_9R(PO_4)_7$ could be prepared for R = Y and Gd−Lu.[15,25] However, $Sr_9R(PO_4)_7$ (R = Y and Tb−Lu) exhibits a monoclinically distorted β-$Ca_3(PO_4)_2$-type structure (space group $I2/a$),[14,25] whereas $Sr_9R(VO_4)_7$ (R = Tm, Yb, and Lu) are isotypic with $Ca_3(VO_4)_2$ (and β-$Ca_3(PO_4)_2$) having space group $R3c$. We may also expect the formation

Table 3. Selected Interatomic Distances (Å) and Bond Valence Sum (BVS) in $Sr_9R(VO_4)_7$ (R = Tm, Yb, and Lu)

	$Sr_9Tm(VO_4)_7$	$Sr_9Yb(VO_4)_7$	$Sr_9Lu(VO_4)_7$
Sr1−O8	2.52(2)	2.455(11)	2.461(9)
Sr1−O10	2.524(11)	2.497(7)	2.496(5)
Sr1−O7	2.56(2)	2.599(11)	2.592(8)
Sr1−O2	2.602(13)	2.618(7)	2.615(6)
Sr1−O6	2.64(2)	2.650(14)	2.645(11)
Sr1−O5	2.70(2)	2.634(12)	2.636(10)
Sr1−O6	2.76(2)	2.640(14)	2.710(11)
Sr1−O4	3.04(2)	3.035(10)	3.026(9)
BVS(Sr1)	1.96	2.11	2.07
Sr2−O2	2.477(14)	2.514(7)	2.514(6)
Sr2−O5	2.48(2)	2.511(9)	2.509(8)
Sr2−O3	2.55(2)	2.571(9)	2.587(7)
Sr2−O4	2.60(2)	2.594(9)	2.585(8)
Sr2−O9	2.63(2)	2.615(14)	2.632(11)
Sr2−O9	2.69(2)	2.736(14)	2.686(12)
Sr2−O8	2.82(2)	2.815(10)	2.836(8)
Sr2−O7	2.88(2)	2.837(11)	2.841(8)
BVS(Sr2)	2.07	2.00	2.00
Sr3−O4	2.53(2)	2.582(10)	2.591(8)
Sr3−O5	2.54(2)	2.535(10)	2.589(8)
Sr3−O7	2.62(2)	2.619(12)	2.600(8)
Sr3−O10	2.70(2)	2.738(12)	2.720(9)
Sr3−O1	2.720(3)	2.709(2)	2.714(2)
Sr3−O10	2.74(2)	2.722(11)	2.738(8)
Sr3−O8	2.77(2)	2.778(10)	2.773(9)
Sr3−O3	2.95(2)	2.914(9)	2.900(7)
Sr3−O2	3.074(14)	2.954(7)	2.960(6)
BVS(Sr3)	1.84	1.84	1.81
Ln−O6 (×3)	2.18(2)	2.231(11)	2.177(8)
Ln−O9 (×3)	2.25(2)	2.203(10)	2.235(8)
BVS(Ln)	3.37	3.20	3.19
V1−O1	1.71(2)	1.679(13)	1.681(9)
V1−O2 (×3)	1.733(11)	1.700(6)	1.698(5)
V2−O3	1.69(2)	1.647(10)	1.651(8)
V2−O4	1.728(14)	1.701(9)	1.709(8)
V2−O5	1.687(14)	1.727(9)	1.702(7)
V2−O6	1.717(13)	1.760(8)	1.759(6)
V3−O7	1.64(2)	1.644(11)	1.673(8)
V3−O8	1.67(2)	1.730(10)	1.716(9)
V3−O9	1.738(13)	1.717(8)	1.721(6)
V3−O10	1.660(14)	1.705(8)	1.687(6)

of solid solutions of $Sr_{9-y}Ca_yR(VO_4)_7$ (R = Tm, Yb, and Lu) for $0 \le y \le 9$ because the boundary compositions are isotypic with each other.[24]

Figure 2 presents plots of χ^{-1} and χ against temperature, *T*, for $Sr_9Tm(VO_4)_7$ and $Sr_9Yb(VO_4)_7$. No noticeable difference was found between the curves measured under the ZFC and FC conditions. These magnetic susceptibility measurements showed that $Sr_9Tm(VO_4)_7$ and $Sr_9Yb(VO_4)_7$ are paramagnetic down to 2 K. The χ^{-1} vs *T* curves were fitted by the Curie−Weiss equation plus the temperature-independent term (χ_0) in the temperature range of 100−400 K:

$$\chi = \chi_0 + C/(T - \Theta) \quad (1)$$

where *C* is the Curie constant and Θ is the Weiss constant. The fitted parameters are given in Table 4. The experimental effective magnetic moments, $\mu_{eff} = (8C)^{1/2}$, were calculated at 7.39 μ_B (μ_B = Bohr magneton) per Tm^{3+} ion and 4.59 μ_B per Yb^{3+} ion. These values are close to the theoretical magnetic moments for the free Tm^{3+} (7.57 μ_B) and Yb^{3+} (4.54 μ_B) ions and to the usually observed values for Tm^{3+} (7.3 μ_B) and Yb^{3+} (4.5 μ_B) ions.[26]

(25) Belik, A. A.; Azuma, M.; Takano, M. *Solid State Ionics* **2004**, *172*, 533.

(26) Kittel, C. *Introduction to Solid State Physics*, 6th ed.; Wiley & Sons: New York, 1986; p 406.

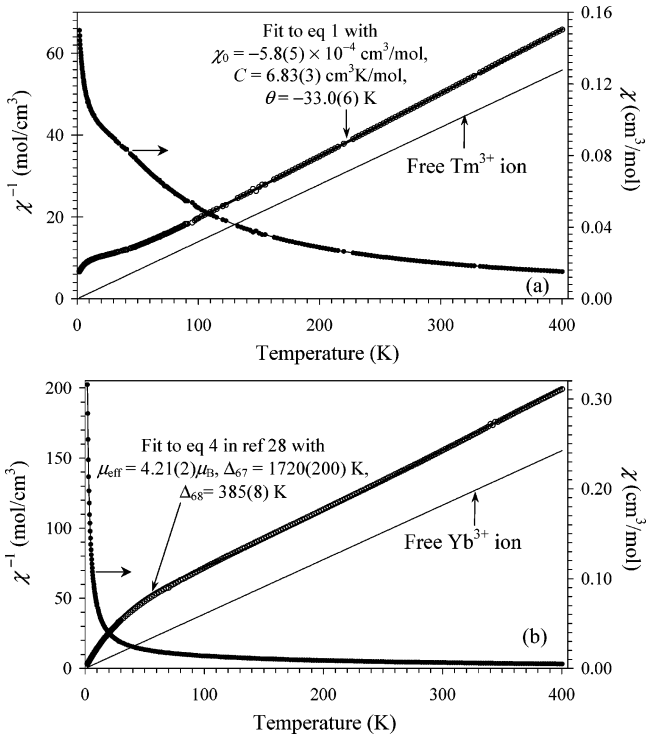

Figure 2. χ^{-1} vs T (empty circles) and χ vs T (black circles) data (ZFC curves; 100 Oe) for (a) $Sr_9Tm(VO_4)_7$ and (b) $Sr_9Yb(VO_4)_7$. Lines for the χ^{-1} vs T curves are the fits to different equations.

Table 4. Fitted Parameters for χ^{-1} vs T and ϵ^{-1} vs T of $Sr_9R(VO_4)_7$ (R = Tm, Yb, and Lu)

		$Sr_9R(VO_4)_7$		
eq	parameter	R = Tm	R = Yb	R = Lu
1	temp range (K)	100−400	100−400	
	χ_0 (cm^3/mol)	$-5.8(5) \times 10^{-4}$	$-4.2(2) \times 10^{-4}$	
	C ((cm^3 K)/mol)	6.83(3)	2.633(11)	
	Θ (K)	−33.0(6)	−85.0(7)	
1	temp range (K)	2−10		
	χ_0 (cm^3/mol)	$8.46(5) \times 10^{-2}$		
	C ((cm^3 K)/mol)	0.290(8)		
	Θ (K)	−2.45(10)		
3	temp range (K)	948−974	948−1000	943−994
	ϵ_0	20(3)	31(2)	39.7(1.4)
	C (K)	$5.63(17) \times 10^3$	$5.56(13) \times 10^3$	$6.17(11) \times 10^3$
	T_0 (K)	929.2(5)	936.6(4)	925.8(3)

Below 100 K, the χ^{-1} vs T curves showed deviations from the Curie−Weiss rule. The χ^{-1} values for $Sr_9Yb(VO_4)_7$ decreased faster with decreasing temperature than those for a free Yb^{3+} ion. $Sr_9Tm(VO_4)_7$ exhibited temperature-independent paramagnetism at low temperatures. Such temperature dependences of χ^{-1} are typical for Tm^{3+} and Yb^{3+} ions affected by an octahedral crystal field.[27]

Below 10 K, the χ^{-1} values for $Sr_9Tm(VO_4)_7$ again started to decrease sharply. This feature might be caused by the presence of paramagnetic impurities or defects. It is known that $Ca_3(VO_4)_2$ has V^{4+} ions (spin 1/2) as defects.[4] However, in the temperature range of 2−10 K, the χ vs T data were fitted by eq 1 with a large Curie constant of 0.290(8) (cm^3 K)/mol (Table 4). Such large C values cannot be assigned to the presence of impurities or defects. In addition, a similar χ^{-1} vs T curve was obtained for $Sr_9Tm(PO_4)_7$. Thus, the sharp

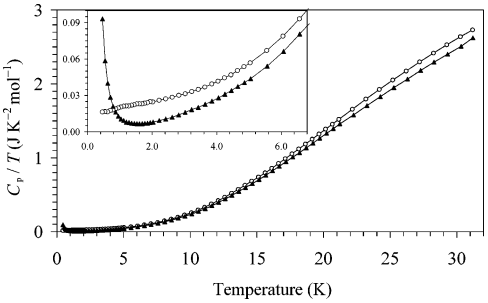

Figure 3. Total specific heat divided by temperature, C_p/T, plotted against T for $Sr_9Tm(VO_4)_7$ (circles) and $Sr_9Yb(VO_4)_7$ (black triangles). The inset gives an enlarged fragment of this figure.

change of χ^{-1} below 10 K should be attributed to the affection of the crystal field.

For the Yb^{3+} ion in an octahedral crystal field, the analytical function for the magnetic susceptibility is given in the literature.[27,28] By fitting the χ^{-1} vs T data for $Sr_9Yb(VO_4)_7$ with the equation given in refs 27 and 28 in the temperature range of 2−400 K, we obtained $\mu_{eff} = 4.21(2)$ μ_B, $\Delta_{67} = 1720(200)$ K, and $\Delta_{68} = 385(8)$ K, where Δ_{68} is the energy difference between the Γ_6 ground state and the first excited state Γ_8 and Δ_{67} is the energy difference between the Γ_6 ground state and the second excited state Γ_7. For other compounds containing octahedrally coordinated Yb^{3+} ions, comparable Δ_{67} and Δ_{68} values were obtained; e.g., $\Delta_{67} = 1762$ K and $\Delta_{68} = 618$ K for Ba_2YbTaO_6[28] and $\Delta_{67} = 1890(140)$ K and $\Delta_{68} = 592(8)$ K for $Sr_9Yb(PO_4)_7$.

Specific heat data showed no anomaly in the temperature range of 0.45−31 K for $Sr_9Tm(VO_4)_7$ (Figure 3). Thus, $Sr_9Tm(VO_4)_7$ does not exhibit any long-range magnetic ordering down to 0.45 K. In other words, the sharp decrease of χ^{-1} below 10 K for $Sr_9Tm(VO_4)_7$ was not caused by a phase transition. For $Sr_9Yb(VO_4)_7$, the sharp upturn in C_p/T was observed below 1.5 K. This fact may indicate the vicinity of the temperature of long-range magnetic ordering. At 2.2−5.5 K, the C_p/T vs T data could be fitted well by the equation

$$C_p/T = \gamma + \beta_1 T^2 + \beta_2 T^4 \qquad (2)$$

with $\gamma \approx 0$ for $Sr_9Yb(VO_4)_7$ but with $\gamma \approx 20.4$ mJ K^{-2} mol^{-1} for $Sr_9Tm(VO_4)_7$. Such behavior of $Sr_9Tm(VO_4)_7$ can be assigned to the Schottky-type contribution owing to the zero-field splitting of the energy levels of Tm^{3+} ions.[29]

No change of mass was detected during the TG measurements of $Sr_9R(VO_4)_7$ (R = Tm, Yb, and Lu) up to 1573 K. Figure 4 presents the DTA curves for the three compounds between 920 and 970 K. In the case of $Sr_9Tm(VO_4)_7$, two peaks were clearly observed during heating (centered at 957 and 961 K) and cooling (centered at 952 and 954 K). For $Sr_9Lu(VO_4)_7$ also double peaks were observed at 952 and 956 K on heating and at 942 and 943 K on cooling. However, $Sr_9Yb(VO_4)_7$ showed a single slightly asymmetric peak centered at 960 K on heating and at 950 K on cooling. The areas of the DTA peaks for the three compounds on heating were close to each other and equal to about 7.0(3) (mV s)/

(27) Dunlap, B. D.; Shenoy, G. K. *Phys. Rev. B* **1975**, *12*, 2716.
(28) Taira, N.; Hinatsu, Y. *J. Solid State Chem.* **2000**, *150*, 31.
(29) Carlin, R. L. *Magnetochemistry*; Springer-Verlag: Berlin, 1986; 327 pp.

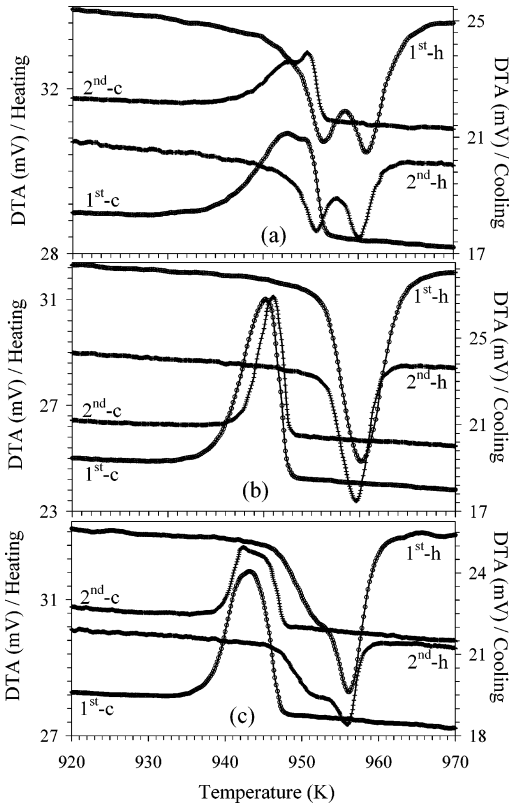

Figure 4. DTA curves for (a) $Sr_9Tm(VO_4)_7$, (b) $Sr_9Yb(VO_4)_7$, and (c) $Sr_9Lu(VO_4)_7$ during heating (h) and cooling (c). Lines with circles are the first (1st) heating−cooling cycle (10 K/min) up to 1273 K, and lines with dashes across them are the second (2nd) heating−cooling cycle (5 K/min) up to 1273 K.

g. All samples remained single-phased after such thermal cycling. No other anomalies on the DTA curves were detected at 300−1573 K. We can assume that two reversible phase transitions of the first order took place in these compounds, with an intermediate phase formed in a very narrow temperature range.

$Sr_9Yb(VO_4)_7$ behaves anomalously (i.e., a single peak on the DTA curves) in comparison with $Sr_9Tm(VO_4)_7$ and $Sr_9Lu(VO_4)_7$. Note that an Yb-specific anomaly was observed in the dependences of the lattice parameters and unit cell volume (V) on the R^{3+} ion size (Table 1);[30] i.e., $Sr_9Yb(VO_4)_7$ has the smallest volume and the smallest a parameter among $Sr_9R(VO_4)_7$ (R = Tm, Yb, and Lu).

At RT, the powder samples (grain size of about 3 μm) of $Sr_9R(VO_4)_7$ (R = Tm, Yb, and Lu) showed SHG signals ~12.5 (R = Tm), ~13.0 (R = Yb), and ~12.0 (R = Lu) times that of quartz. This fact proved that they crystallize in the noncentrosymmetric space group at RT. Note that the ceramic samples, i.e., with a larger grain size, demonstrated larger SHG signals 100−120 times that of quartz. The temperature dependence of the SHG signals is presented in Figure 5 for $Sr_9Lu(VO_4)_7$ as an example. The SHG signals decreased with increasing temperature and then disappeared sharply at the critical temperature, which coincides with the anomaly on the DTA curves. This fact indicated that the high-temperature phases of $Sr_9R(VO_4)_7$ (R = Tm, Yb, and Lu) possess the center of symmetry. On cooling, we observed

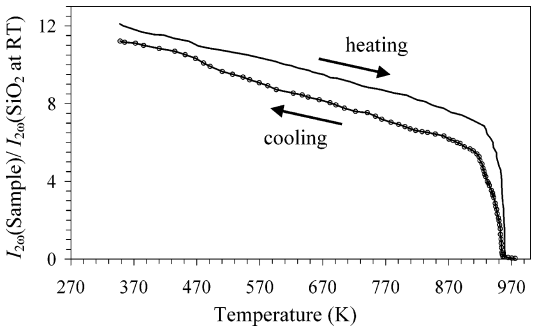

Figure 5. Temperature dependence of the SHG signals for $Sr_9Lu(VO_4)_7$ during heating and cooling.

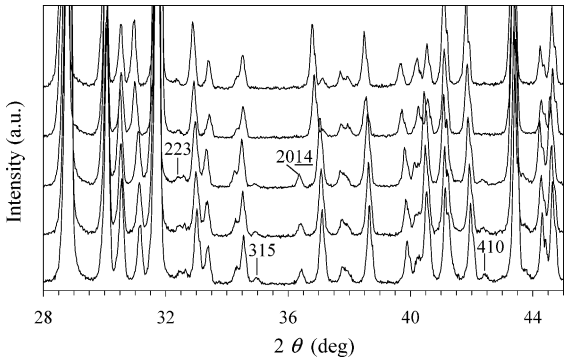

Figure 6. Fragments of the temperature dependence of the XRD patterns for $Sr_9Lu(VO_4)_7$. From the bottom to the top: 709, 796, 883, 970, and 1057 K. Indices for some reflections are given.

a small hysteresis. The presence of hysteresis and the stepwise disappearance of the SHG signal are characteristic of a first-order phase transition.

The temperature dependence of the XRD patterns for $Sr_9Lu(VO_4)_7$ is given in Figure 6. We have found that all reflections with odd indices l disappeared in the high-temperature phase. Note that the intensities of some other reflections also changed noticeably after the phase transition, e.g., for the (2,0,14) reflection. Thus, for the high-temperature phase, the c parameter seems to be reduced by a factor of 2. With lattice parameters of $a \approx 11.3$ Å and $c \approx 20.2$ Å, the reflection conditions were $-h + k + l = 3n$ for $hkil$, $h + l = 3n$ for $h\bar{h}0l$, and $l = 3n$ for $hh\bar{2}hl$ (hexagonal axes, obverse setting), affording possible space groups $R3$, $R\bar{3}$, $R32$, $R3m$, and $R\bar{3}m$.[31] Taking into account the results of the high-temperature SHG measurements, we selected a centrosymmetric space group with maximum symmetry (that is, $R\bar{3}m$) for the high-temperature phases of $Sr_9R(VO_4)_7$ (R = Tm, Yb, and Lu). Note that high-temperature modifications of $Sr_9R(PO_4)_7$ (R = Sc, Cr, Fe, Ga, Y, In, and Gd−Lu) and $Sr_9NiLi(PO_4)_7$ also crystallize in space group $R\bar{3}m$ with the same lattice dimensions.[25]

Figure 7 shows the temperature dependence of lattice parameters (a, c/Z, and V/Z) for $Sr_9Tm(VO_4)_7$ and $Sr_9Lu(VO_4)_7$. The phase transitions were accompanied by a stepwise decrease of the a parameter and a stepwise increase of the c/Z parameter as expected from the nature of the first-order phase transition.

(30) Shannon, R. D. *Acta Crystallogr., Sect. A: Found. Crystallogr.* **1976**, *32*, 751.

(31) *International Tables for Crystallography*, 5th ed.; Hahn, T., Ed.; Kluwer: Dordrecht, The Netherlands, 2002; Vol. A, p 52.

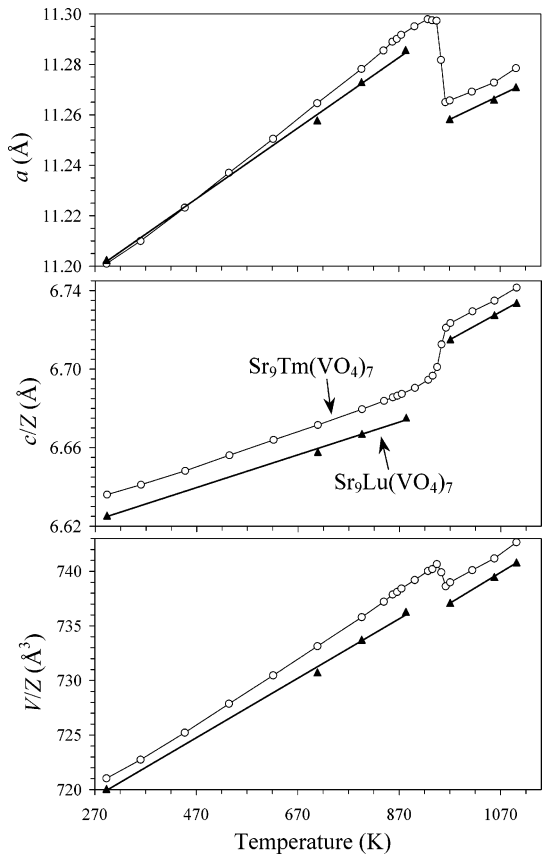

Figure 7. Temperature dependence of lattice parameters (*a*, *c*/*Z*, and *V*/*Z*) for $Sr_9Tm(VO_4)_7$ (circles) and $Sr_9Lu(VO_4)_7$ (black triangles).

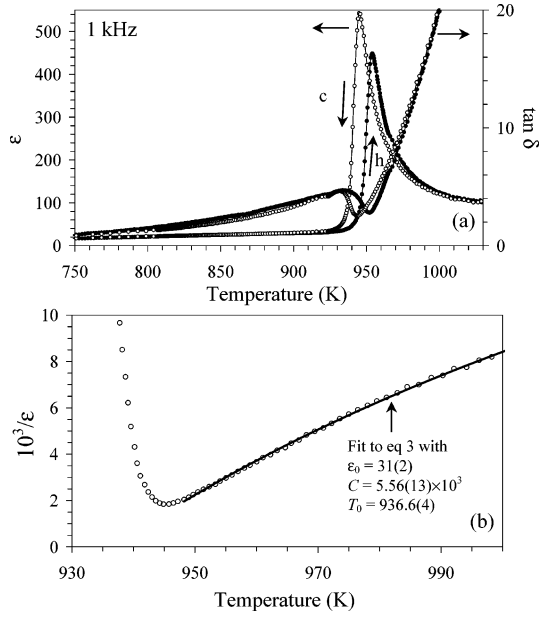

Figure 8. (a) Temperature dependence of the dielectric permittivity and tangent losses at 1 kHz for $Sr_9Yb(VO_4)_7$ during heating and cooling. (b) Temperature dependence of the inverse dielectric permittivity during cooling at 1 kHz for $Sr_9Yb(VO_4)_7$ (circles) with the Curie−Weiss fit (solid line).

Figure 8 depicts the temperature dependence of ϵ, ϵ^{-1}, and tan δ at 1 kHz for $Sr_9Yb(VO_4)_7$ as an example. The very sharp maxima (ϵ_{max}) at the characteristic temperature, T_c, on the ϵ vs T curves and the anomaly on the tan δ vs T curves just below T_c suggested that $Sr_9R(VO_4)_7$ (R = Tm, Yb, and Lu) undergo a ferroelectric−paraelectric phase transition. No frequency dependence of T_c was found. Above T_c, the ϵ^{-1} vs T curves obeyed the Curie−Weiss law:

$$\epsilon = \epsilon_0 + C/(T - T_0) \quad (3)$$

The fitted parameters are given in Table 4. These facts indicate that $Sr_9R(VO_4)_7$ (R = Tm, Yb, and Lu) behave as classical (not relaxer) ferroelectrics.[32]

It is known that the related compounds $Ca_3(VO_4)_2$[1] and $Ca_9R(VO_4)_7$ (R = La−Lu and Bi)[9] are ferroelectric. A proper ferroelectric−paraelectric phase transition in crystals with a rhombohedral symmetry should take place keeping the unit cell dimensions essentially the same.[33] However, the low-temperature phase of $Sr_9R(VO_4)_7$ (R = Tm, Yb, and Lu) has unit cell dimensions of $a \approx 11.3$ Å and $c \approx 40.1$ Å (space group $R3c$), whereas the high-temperature phase has $a \approx 11.2$ Å and $c \approx 20.2$ Å (space group $R\bar{3}m$). This fact also suggests the existence of an intermediate phase.

Thus, we can propose the following sequential transitions: $R3c$ ($a \approx 11.3$ Å and $c \approx 40.1$ Å) ⇒ $R\bar{3}c$ ($a \approx 11.3$ Å and $c \approx 40.1$ Å) ⇒ $R\bar{3}m$ ($a \approx 11.3$ Å and $c \approx 20.2$ Å) or $R3c$ ($a \approx 11.3$ Å and $c \approx 40.1$ Å) ⇒ $R3m$ ($a \approx 11.3$ Å and $c \approx 20.2$ Å) ⇒ $R\bar{3}m$ ($a \approx 11.3$ Å and $c \approx 20.2$ Å). The first step in the former sequence and the second step in the latter sequence proceed without changing the unit cell dimensions significantly, fulfilling the requirement of a simple ferroelectric−paraelectric phase transition. The steps other than these may be usual structural phase transitions.[33] Because the intermediate phase exists in a very narrow temperature range, it is very difficult to determine its real symmetry with high-temperature XRD and other methods.

A somewhat similar situation was observed in the case of ferroelectric−paraeletric phase transitions in Aurivillius phases $Sr_{0.85}Bi_{2.1}Ta_2O_9$[34] and $SrBi_2Nb_2O_9$,[35,36] which are structurally very close to each other. $Sr_{0.85}Bi_{2.1}Ta_2O_9$ undergoes a ferroelectric−paraeletric phase transition ($A2_1am$ ⇒ $Amam$) without a noticeable change in unit cell dimensions. The $Amam$ phase then transforms to an $I4/mmm$ phase which has a unit cell of half the volume of the ferroelectric $A2_1am$ phase. On the other hand, for $SrBi_2Nb_2O_9$, the intermediate $Amam$ phase was not detected with power diffraction methods, and a direct $A2_1am$ to $I4/mmm$ transformation was proposed.[35] In a similar way, we can say that the low-temperature phase of $Sr_9Yb(VO_4)_7$ transforms to the high-temperature phase directly as suggested from the DTA results.

When $Sr_9R(VO_4)_7$ (R = Tm, Yb, and Lu) were heated very fast above the phase transition temperatures (in 2−3 min), we observed a macroscopic phase separation. The samples contained a phase with lattice parameters of $a \approx$

(32) Ravez, J. *C. R. Acad. Sci. Paris, Ser. IIc: Chim.* **2000**, 267.
(33) See for example, Lonkai, Th.; Tomuta, D. G.; Amann, U.; Ihringer, J.; Hendrikx, R. W. A.; Többens, D. M.; Mydosh, J. A. *Phys. Rev. B* **2004**, *69*, 134108.
(34) Hervoches, C. H.; Irvine, J. T. S.; Lightfoot, P. *Phys. Rev. B* **2001**, *64*, 100102(R).
(35) Snedeen, A.; Hervoches, C. H.; Lightfoot, P. *Phys. Rev. B* **2003**, *67*, 092102.
(36) Shimakawa, Y.; Imai, H.; Kimura, H.; Kimura, S.; Kubo, Y.; Nishibori, E.; Takata, M.; Sakata, M.; Kato, K.; Hiroi, Z. *Phys. Rev. B* **2002**, *66*, 144110.

11.3 Å and $c \approx 40.1$ Å (space group $R3c$ or $R\bar{3}c$) and a phase with lattice parameters of $a \approx 11.2$ Å and $c \approx 20.2$ Å (space group $R3m$ or $R\bar{3}m$). Two small reflections due to unknown impurities also appeared on the synchrotron XRD patterns in this case. The phase separation disappeared even when the sample was cooled rapidly.

The high-temperature XRD data in Figure 6, however, proved that no macroscopic phase separation took place when the samples were heated slowly (10 K/min). No dramatic increase of the full width at half-maximum of reflections in the XRD patterns was observed in this case. The good reproducibility of the DTA curves taken with different heating−cooling rates also indicated that the two peaks observed on the DTA curves were due to the thermodynamic phase transitions, not caused by phase separation or decomposition.

In conclusion, we showed that $Sr_9R(VO_4)_7$ with R = Tm, Yb, and Lu possess the $Ca_3(VO_4)_2$-type structure. The structure parameters were refined from the synchrotron XRD data. We also characterized the three compounds by the magnetic susceptibility, the specific heat, thermal analysis, and high-temperature X-ray powder diffraction, second-harmonic generation, and dielectric measurements. Every one of these compounds exhibits a high-temperature phase transition of the first order near 950−960 K which has characteristics of a ferroelectric−paraelectric phase transition. The low-temperature phase with $R3c$ symmetry transforms to the high-temperature phase with $R\bar{3}m$ symmetry through an intermediate phase.

Acknowledgment. We express our thanks to the Ministry of Education, Culture, Sports, Science and Technology, Japan, for Grant-in-Aid No. 12CE2005, for COE Research on Elements Science (Grant Nos. 13440111 and 14204070), and for 21COE to the Kyoto Alliance for Chemistry. The synchrotron radiation experiments were performed at SPring-8 with the approval of the Japan Synchrotron Radiation Research Institute. We thank the staff of beam line BL02B2 at SPring-8 for technical assistance. This work was also partially supported by the Russian Foundation for Basic Research (Grant 04-03-32417).

Supporting Information Available: Phase composition of some samples with the nominal composition of $Sr_9R(VO_4)_7$ (R = Y and La−Er) (Table S1), observed, calculated, and difference synchrotron XRD patterns of $Sr_9Tm(VO_4)_7$ and $Sr_9Lu(VO_4)_7$ at RT (Figure S1), experimental synchrotron XRD pattern of $Sr_9Nd(VO_4)_7$ at RT (Figure S2), temperature dependence of the dielectric constants, tangent losses, and inverse dielectric constants with the Curie−Weiss fit for $Sr_9R(VO_4)_7$ (R = Tm, Yb, and Lu) (Figure S3), temperature dependence of the SHG signals in $Sr_9R(VO_4)_7$ (R = Tm and Yb) (Figure S4), fragments of observed, calculated, and difference synchrotron XRD patterns of $Sr_9Yb(VO_4)_7$ at RT and 973 K (Figure S5), and angular dependence of the full width at half-maximum of reflections on XRD patterns for $Sr_9Lu(VO_4)_7$ at different temperatures (Figure S6) (PDF). This material is available free of charge via the Internet at http://pubs.acs.org.

CM048282F